Vol. 495: 77–90, 2014
doi: 10.3354/meps10559

MARINE ECOLOGY PROGRESS SERIES
Mar Ecol Prog Ser

Published January 9

Evidence for light-environment control of carbon isotope fractionation by benthic microalgal communities

Kara R. Radabaugh*, Elon M. Malkin, David J. Hollander, Ernst B. Peebles

University of South Florida, College of Marine Science, St. Petersburg, Florida 33701, USA

ABSTRACT: Assemblages of filamentous algae and diatoms were grown on glass plates suspended in the water column in Tampa Bay, Florida (USA). Carbon isotope ratios ($\delta^{13}C$) of the accumulated OM (OM) were analyzed to compare the effects of aqueous CO_2 concentration, OM accumulation rate, algal type, and photosynthetically active radiation (PAR) on community-level carbon isotope fractionation between aqueous CO_2 and organic carbon. Concentrations of nutrients, PAR, and colored dissolved OM exhibited spatiotemporal variation during 6 experiments conducted over 2 mo of variable rainfall and terrestrial runoff. Fractionation ranged from 6.8 to 13.7‰ and was positively correlated with PAR, resulting in higher $\delta^{13}C$ values for OM in low-light conditions. Fractionation was lower and OM accumulation rates were higher during the 3 early experiments, which had high nutrient concentrations as a result of terrestrial runoff. OM accumulation rates and CO_2 concentrations did not independently correlate with fractionation. The dominant factors influencing fractionation were PAR and spatial coverage by pennate diatoms, which together explained 56% of variability in fractionation. These results indicate that PAR significantly influences microalgal fractionation in estuaries, supporting the concept that the light environment may contribute to the widely observed phenomenon of higher $\delta^{13}C$ values in benthic algae relative to phytoplankton.

KEY WORDS: Photosynthetic fractionation · Benthic algae · Basal resource · Light attenuation · Estuary

INTRODUCTION

Numerous laboratory experiments have been conducted to isolate the causes of variation in carbon isotope photosynthetic fractionation (ε_p) by aquatic microalgae. These experiments have shown that algal growth rate, aqueous CO_2 concentration [CO_2(aq)], cell geometry (surface area to volume ratio), and light intensity can each cause substantial variations in ε_p (Laws et al. 1997, Popp et al. 1998, Rost et al. 2002). Simultaneous variation and interaction among these potentially influential factors complicates the explanation and prediction of ε_p (Bade et al. 2006). This raises the question as to which of these pertinent responses dominates under natural conditions.

Understanding carbon isotope fractionation is essential to analysis of biomass pathways. Variations in $\delta^{13}C$ values of primary producers are used in ecological studies to trace trophic biomass linkages between primary producers (basal resources) and consumers. In most freshwater and coastal ecosystems, the principal basal resources used in isotopic mixing models are phytoplankton, benthic algae, and vascular plants (e.g. Haines & Montague 1979, Thorp et al. 1998, Kharlamenko et al. 2001). In shallow marine and estuarine waters, the average $\delta^{13}C$ values of benthic algae are ~5‰ higher than phytoplankton, providing an isotopic tracer for differentiating between dependence on planktonic and benthic basal resources (France 1995, Doi et al. 2010).

*Corresponding author: kradabau@mail.usf.edu

Unlike the laboratory experiments that have investigated ε_p using isolated species of phytoplankton or benthic algae, investigations of trophic linkages in natural settings typically must consider a complex assemblage of microalgal species that includes variable amounts of other organic matter (OM) (Haines & Montague 1979, Thorp et al. 1998, Kharlamenko et al. 2001, Radabaugh & Peebles 2012). The $\delta^{13}C$ signature of these communities depends upon $\delta^{13}C$ values of dissolved inorganic carbon (DIC), community species composition, and the magnitude of ε_p by primary producers within these assemblages. Interaction among potentially influential factors complicates prediction of algal ε_p in natural settings (Riebesell et al. 2000, Bade et al. 2006).

Here we investigated community-level fractionation (ε) between aqueous CO_2 and an OM assemblage representative of a benthic algal community. This community-level carbon fractionation is denoted by the ε symbol rather than by ε_p to acknowledge other non-microalgal organisms and OM that were present in small amounts during the experiments. The objective of the present study was to determine whether OM accumulation rate, algal composition, light, or [CO_2(aq)] dominated control of ε and $\delta^{13}C$ values in a naturally variable estuarine setting.

OVERVIEW OF PHOTOSYNTHETIC FRACTIONATION

During photosynthesis, the lighter ^{12}C isotope is preferentially utilized for carbon fixation over ^{13}C, resulting in lower $\delta^{13}C$ values of photosynthate relative to ambient CO_2. Carbon fractionation by aquatic microalgae occurs during uptake of CO_2 into the cell and during carbon fixation by carboxylase enzymes (Goericke et al. 1994, Fry 1996). Experiments in the field and laboratory have shown that low algal growth rate and high [CO_2(aq)] each result in higher ε_p (Fry & Wainright 1991, Hollander & McKenzie 1991, Freeman & Hayes 1992, Riebesell et al. 2000). Specific growth rate (μ) and [CO_2(aq)] are frequently paired as a ratio to examine the relationship between ε_p and $\mu/[CO_2(aq)]$ (Bidigare et al. 1997, Popp et al. 1998). The ε_p versus $\mu/[CO_2(aq)]$ relationship may vary depending on algal species and the growth-limiting factor (Popp et al. 1998, Cassar et al. 2006).

The magnitude of algal ε_p is also influenced by species composition and boundary-layer thickness. Surface area to volume ratios of algal cells affect rates of influx and demand for intracellular carbon; nutrient or carbon uptake strategies also vary among algal species (Fry & Wainright 1991, Popp et al. 1998, Burkhardt et al. 1999). In the thin, stagnant boundary layer between algal cells and the adjacent water, CO_2 and HCO_3^- are transported by molecular diffusion rather than by turbulent transfer (Smith & Walker 1980, France 1995). Algae remove CO_2 during photosynthesis, resulting in lower [CO_2(aq)] within the boundary layer compared to the adjacent water. The higher $\delta^{13}C$ values of benthic algae have been attributed to this boundary-layer effect (Smith & Walker 1980, France 1995).

Light has also been shown to have a positive relationship with ε_p. This trend is difficult to study as light and growth rate are inherently linked, yet have opposing effects on ε_p, creating offsetting trends that may mask relative contributions to ε_p (Riebesell et al. 2000, Rost et al. 2002). Under controlled laboratory conditions, both the coccolithophore *Emiliania huxleyi* and the marine diatom *Phaeodactylum tricornutum* exhibited much greater ε_p under high-light conditions (Riebesell et al. 2000, Rost et al. 2002). Continuous light also resulted in greater ε_p by diatoms and *E. huxleyi* compared to algae grown in shorter photoperiods (Burkhardt et al. 1999, Rost et al. 2002).

Light is thought to influence algal ε_p through a carbon concentrating mechanism (CCM), as the ATP yielded during photochemical reactions may provide the energy needed for active uptake of inorganic carbon (Riebesell et al. 2000, Rost et al. 2002). The CCM may increase carbon influx into the cell at a rate faster than carbon fixation, resulting in greater isotopic discrimination during carbon fixation (Burns & Beardall 1987, Rotatore et al. 1992, Rost et al. 2002). The CCM could operate by several possible pathways: active uptake of CO_2, uptake of HCO_3^- with intracellular conversion to CO_2 via various carbonic anhydrases, or by extracellular conversion of HCO_3^- to CO_2 followed by diffusive or active uptake of CO_2 (Burns & Beardall 1987, Hayes 1993, Laws et al. 1997). If cells actively uptake HCO_3^- rather than CO_2, the inorganic carbon source will have higher $\delta^{13}C$ values due to the equilibrium fractionation between CO_2 and HCO_3^- in seawater (Mook et al. 1974).

MATERIALS AND METHODS

Experimental setup

The apparatus in Fig. 1 was deployed in an average total water depth of 2.7 m in Bayboro Harbor on the western side of Tampa Bay, Florida, USA (27.760° N,

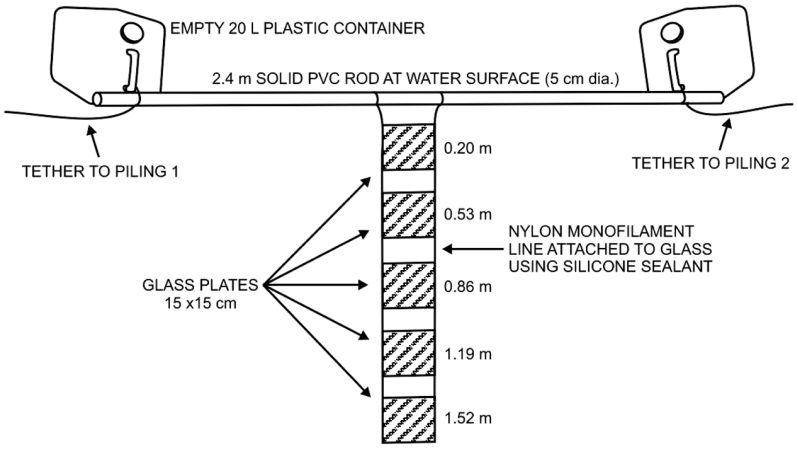

Fig. 1. Apparatus used to accumulate algae-dominated organic matter at constant depths in the water column. Average total water depth was 2.7 m. Plate-growing surfaces were approximately oriented along the northwest–southeast axis

82.633° W). Bayboro Harbor receives terrestrial runoff from residential areas within metropolitan St. Petersburg. Variable freshwater input and occasional stratification at the study site provide diverse water conditions in which to study the factors influencing carbon isotope fractionation. The small, triangular bay is surrounded by buildings on 3 sides and is relatively protected from the stronger wind, waves, and currents in Tampa Bay. The depth at which the plates were suspended was constant, as the buoyant containers rose and fell with the 0.3 to 0.7 m tide.

Six deployments (5 to 8 d each) of this apparatus (experiments) were conducted during an 8 wk period from 13 May to 7 July 2009 that coincided with the typical annual transition from the late winter/spring dry season to the summer rainy season. At the start, middle, and end of each experiment, vertical water-quality profiles were obtained using a multisensor platform. All measurements were made between 09:00 and 11:30 h with the exception of 2 bad-weather days during Expt 1 when measurements were made in the early afternoon.

The multisensor platform included a pre- and post-calibrated YSI sonde (6920V2-2) for measuring temperature, salinity, chlorophyll fluorescence, depth, and pH. A WET Labs ECO Triplet on the platform provided profiles of colored dissolved organic matter (CDOM) fluorescence (Ex/Em of 370/460 nm), and a Walz Diving pulse-amplitude-modulated (PAM) fluorometer contained a photosynthetically active radiation (PAR) sensor. A remotely controlled, stainless-steel well pump was used to collect water samples from ~0.2, 0.85, and 1.5 m depths for water analyses and instrument calibration.

Because the instrument readings, water samples, and OM data were obtained using different temporal and depth resolutions, high frequency (1 Hz) sampling values from the sonde and ECO Triplet were averaged from the start, middle, and end of each experiment (5 to 8 d) to represent average conditions at the 5 depths occupied by the glass plates. This enabled comparison of average water-column data with OM data at the same depth resolution.

At the end of each experiment, the glass plates were removed from the water and replaced by new glass plates so no material would be retained between experiments. The accumulated growth was examined by light microscopy to visually estimate percent cover on the glass plate by centric diatoms, pennate diatoms with associated mucilage, filamentous algae, and cnidarian polyps. The percent coverage values for each organism type were binned into 6 cover classes in order to compensate for error associated with visual estimation, reflecting methods used for classification of vegetation canopy coverage (Daubenmire 1959, Floyd & Anderson 1987). Percent coverage ranges for the cover classes were 0–5, 5–25, 25–50, 50–75, 75–95, and 95–100% coverage. The midpoints of the cover classes (2.5, 15, 37.5, 62.5, 85, 97.5) were used to describe coverage of each organism type. Midpoints were treated as a quantitative rather than categorical variable in statistical analyses.

Isotopic analyses

The accumulated OM was scraped off individual glass plates using a glass microscope slide, acidified with 0.1 M HCl to remove inorganic carbon, and thoroughly rinsed with deionised water onto a 35 µm Nitex mesh sieve. Biomass in the retained fraction (>35 µm) was dried at 50°C for 48 h and homogenized using a mortar and pestle. Net OM accumulation rate (A_{OM}) of the >35 µm size fraction was calculated as µg dry weight cm^{-2} d^{-1}.

$^{13}C/^{12}C$ was measured in duplicate on an elemental analyzer (EA Carlo-Erba NA2500 Series II) coupled to a continuous flow isotopic ratio mass spectrometer (IRMS ThermoFinnigan Delta+XL) at the University of South Florida College of Marine Science in St. Petersburg, Florida. Calibrating standards were NIST 8573 and NIST 8574 L-glutamic acid Standard

Reference Materials. Analytical precision, obtained by replicate measurements of NIST 1570a spinach leaves, was −27.28 ± 0.19‰ for $\delta^{13}C$ (average standard deviation of 44 samples). All $\delta^{13}C$ values are reported relative to the Pee Dee Belemnite standard (PDB):

$$\delta^{13}C_{sample} = 1000\left[\frac{\left(^{13}C/^{12}C\right)_{sample}}{\left(^{13}C/^{12}C\right)_{PDB}} - 1\right] \quad (1)$$

As this study focuses on community-level stable isotopic analysis, carbon isotope fractionation is denoted as ε in order to clarify that this fractionation factor is determined from $\delta^{13}C$ values of an algae-dominated community, rather than pure photosynthetic fractionation by isolated phytoplankton cells (ε_p). ε calculations were modeled after ε_p (Freeman & Hayes 1992, Burkhardt et al. 1999):

$$\varepsilon = (\delta^{13}C_{CO2} - \delta^{13}C_{OM}) / (1 + \delta^{13}C_{OM} / 1000) \quad (2)$$

where $\delta^{13}C_{CO2}$ and $\delta^{13}C_{OM}$ are the $\delta^{13}C$ values of dissolved aqueous CO_2 and OM, respectively. While the fractionation process results in $\delta^{13}C_{OM}$ values that are more negative than those of $\delta^{13}C_{CO2}$, the calculated ε is reported as a positive value.

Water samples for $\delta^{13}C$ values of DIC ($\delta^{13}C_{DIC}$) were fixed with $HgCl_2$ solution and stored in sealed, glass-stoppered containers without headspace. A 12 ml exetainer containing 3 drops of phosphoric acid (H_3PO_4) was sealed and purged with helium. One ml of sample was added via syringe, and the headspace was allowed to stabilize for 13 h at room temperature before measurement. A sample of CO_2 was carried via a Thermo Finnigan Gas Bench II to the IRMS. $\delta^{13}C_{CO2}$ was calculated from $\delta^{13}C_{DIC}$ using the equation

$$\delta^{13}C_{CO2} = \delta^{13}C_{DIC} + 23.644 - (9701.5 / T_k) \quad (3)$$

where T_k is the *in situ* water temperature in degrees Kelvin (Mook et al. 1974, Rau et al. 1996).

Water quality analyses

Water samples for calculation of $[CO_2(aq)]$ were fixed with $HgCl_2$ solution and stored in sealed, glass-stoppered containers without headspace. Sample aliquots (20 ml) were acidified with 10 ml of 3 M H_3PO_4, and the concentration of total DIC (C_T) was then measured by coulometer (UIC CM 5014) against certified reference materials (CRM) from the laboratory of A. Dickson (Scripps Institute of Oceanography). The standard deviation for 9 CRM C_T measurements was ±8.6 µmol kg^{-1} seawater (SW). Akalinity (A_T) was measured on an HP 8453 spectrometer using bromocresol purple according to the method described by Yao & Byrne (1998). The A_T standard deviation for 3 CRM measurements was ±1.5 µmol kg SW^{-1}.

$[CO_2(aq)]$ was calculated from C_T and A_T for 47 water samples using the CO2SYS Excel program of Pierrot et al. (2006) and the dissociation constants of Mehrbach et al. (1973) as modified by Dickson & Millero (1987). The uncertainty for calculated $[CO_2(aq)]$ was determined by Monte Carlo simulation of CRM measurements. The standard deviations of C_T and A_T mentioned above were used to create normally distributed C_T and A_T data sets; the MATLAB version of CO2SYS was then used to calculate CRM $[CO_2(aq)]$ 100 000 times based upon these distributions of C_T and A_T. The standard deviation of the calculated $[CO_2(aq)]$ values was 0.7 µmol kg SW^{-1} (±4.4%).

Accurate A_T data were not available for 2 water samples due to excessive addition of acid during the alkalinity titration; in these cases $[CO_2(aq)]$ was calculated from C_T and YSI pH measurements. For 6 additional samples, $[CO_2(aq)]$ was calculated from A_T and pH, rather than C_T, due to poor coulometer performance on the day these samples were analyzed. On days when pH was used for $[CO_2(aq)]$ calculations, post-calibration accuracy of the YSI pH sensor was 7.02 ± 0.06 pH units. The pH from the YSI sonde was calibrated on the total pH scale by comparing YSI pH values to total scale pH calculations from C_T and A_T using CO2SYS. Temperature changes were accounted for by increasing the pH by 0.0143 units for every 1°C decrease in temperature between *in situ* and laboratory calibration conditions. YSI pH was lowered by 0.138 units in order to minimize the residual sum of squares between YSI pH values and total scale pH values calculated in CO2SYS.

Water samples for nutrient analysis were filtered through a 20 µm membrane filter and frozen; all samples were analyzed within 6 mo. Nitrate + nitrite, silicate, ammonium, and phosphate were measured on a Technicon-Autoanalyzer II segmented flow analyzer according to Gordon et al. (1993).

Water samples for CDOM calibration were immediately filtered through 0.2 µm nylon membrane filters and frozen until analysis. Absorbance ($D(\lambda)$) was measured from 200 to 800 nm wavelengths (λ) in a 10 cm cuvette on a Perkin Elmer Lambda 18 or Lambda 25 spectrometer. Absorption coefficients ($a(\lambda)$, in units of m^{-1}) were calculated as

$$a(\lambda) = 2.303\, D(\lambda) / L \quad (4)$$

where L is the cuvette path length (10 cm). Absorption at 700 nm was subtracted to produce null-corrected absorption. CDOM fluorescence readings from the ECO Triplet were calibrated against a(440). The exponential slope of the absorption curve (S) was calculated as

$$a(\lambda) = a(\lambda_0)e^{-S(\lambda - \lambda_0)} \quad (5)$$

where $\lambda = 600$ nm and $\lambda_0 = 400$ nm.

Chlorophyll samples were immediately filtered onto GF/F glass microfiber filters and frozen at −80°C until extraction. Chlorophyll concentration was determined fluorometrically (Holm-Hansen & Riemann 1978). Filters were extracted in 10 ml of methanol over 24 h in a freezer, sonicated for 30 s, and centrifuged for 5 min at ~1000 × g, and fluorescence was then measured on a Turner Designs 10-AU fluorometer.

Calculation of PAR

Direct PAR measurements in the water column were obtained using a PAR sensor on the Diving-PAM, but were not used for analysis due to interference from variation in water-surface smoothness, patchy cloudiness, and irregular shading by the other instruments. Instead, HydroLight version 5 (Mobley & Sundman 2008) was used to calculate depth-specific vertical light attenuation coefficients (K_d) for the sampling dates in the experimental time period. K_d is defined as the change in downward irradiance, E_d, over change in water depth, dz (Kirk 1994):

$$K_d = -\mathrm{d} \ln E_d / \mathrm{d}z \quad (6)$$

PAR is attenuated underwater by absorption and scattering by phytoplankton, CDOM, suspended particulates, and water molecules (Kirk 1994). The HydroLight model was run for Case 2 waters; see HydroLight 5 technical documentation for details on K_d calculation (Mobley & Sundman 2008). Default water absorption (Pope & Fry 1997) and scatter coefficients (Morel 1974) were used in the HydroLight model. Average mass-specific chlorophyll and detrital absorption coefficients were obtained from spectral data from Bayboro Harbor during May to July of 2004 and 2005 (Du 2005). Backscatter for chlorophyll and mineral components were based upon Gordon & Morel (1983) HydroLight defaults. Depth-specific chlorophyll concentrations and CDOM absorptions at 400 nm, calibrated as mentioned above, were included in the model. The absorption spectra for CDOM were provided using date-specific slopes (Eq. 5).

Light attenuation of PAR, K_d(PAR), was calculated at zenith in the HydroLight model and adjusted hourly according to solar angle:

$$K_d'(\mathrm{PAR}) = K_d(\mathrm{PAR}) / \cos(\theta) \quad (7)$$

where θ is the zenith angle of light underwater (Kirk 1994). Location-specific PAR was calculated for each daylight hour during the experiments. These values were compared to above-water measurements from the Diving-PAM PAR sensor on cloudless days to ensure they were within a similar range. This PAR value was reduced for the percentage of cloud cover based on values from Kirk (1994); cloud data were obtained from a nearby meteorological station at Albert Whitted Airport in St. Petersburg. Surface reflectance was calculated for each hour from Fresnel's equation of reflectance using the solar angle (Kirk 1994). Depth-specific PAR was calculated from these values using K_d'(PAR) for every hour and integrated throughout the day, resulting in total PAR per day (mol m^{-2} d^{-1}). Daily PAR was averaged for each 5 to 8 d experiment.

Statistical analyses

Median values of parameters from the 3 early experiments (13 May to 12 June) and 3 later experiments (12 June to 7 July) were compared using Mann-Whitney U (Wilcoxon rank sum) tests. To determine which variables explained the most variability in ε, factors known to influence photosynthetic fractionation were included in a generalized linear regression. Included variables were PAR, [NO_3+NO_2 +NH_4], A_{OM}, [CO_2(aq)], and cover classes for pennate diatoms, centric diatoms, and filamentous algae. Inorganic N:P was <4 throughout the experiments; thus [PO_4] was not included in model selection. The Akaike Information Criterion (AIC) and ΔAIC (difference between the current model and the model with the lowest AIC value) were calculated for models containing all possible combinations of variables (Burnham & Anderson 2002). The model with the lowest (best) AIC value was selected for graphical display. The variance inflation factor (VIF) was calculated to determine the degree of multicollinearity within the model (O'Brien 2007). The VIF is calculated as the reciprocal of tolerance:

$$\mathrm{VIF} = 1 / (1 - R_i^2) \quad (8)$$

where R_i^2 is the proportion of variance in the ith independent variable that is related to the other variables in a multiple regression (O'Brien 2007). A low

VIF indicates that the model is acceptable and not impacted by multicollinearity. All statistical analyses were performed using Statgraphics Centurion XVI.

RESULTS

Environmental conditions

Rainfall was heaviest during the early and later parts of the study (Fig. 2). The rainfall that occurred during the first experiment (13–21 May) was the first substantial precipitation to occur in the area for 28 d preceding the experiment. The freshwater runoff from this initial precipitation of the rainy season led to stratified conditions at the experiment site. The low salinity surface layer had high nutrient and CDOM concentrations (Fig. 2). The concentrations of CDOM, nitrate + nitrite, ammonium, and silicate exhibited significant positive correlations with each other and were negatively correlated with salinity (correlation p-values < 0.05; see Table A1 in the Appendix for nutrient concentrations). The magnitude of these vertical water-quality fluctuations was reduced when averaged over the 5 to 8 d experiments (Table 1). Average weekly values are depicted in Fig. 3.

In spite of high precipitation in late June and early July, the high-nutrient, high-CDOM surface layer was less pronounced during the latter half of the experimental period (Fig. 2). The median values of environmental parameters were compared between the early 3 experiments (13 May to 12 June 2009) and the later 3 experiments (12 June to 7 July) using Mann-Whitney *U*-tests (Table 2). The early experiments had significantly higher median concentrations of NO_3+NO_2 and CO_2(aq) (Table 2).

Calculated PAR in the water column varied as a result of cloud cover and light attenuation by CDOM and phytoplankton (Fig. 2). The range of K_d(PAR) was 0.30 to 1.11 m^{-1} during the experiments, which is consistent with light attenuation values in previous Tampa Bay studies (McPherson & Miller 1994). Average PAR during the experiments ranged from 33.8 to 46.6 mol m^{-2} d^{-1} at the depth of the shallowest plate (0.2 m) and from 17.4 to 26.4 mol m^{-2} d^{-1} at the deepest plate (1.52 m; Table 1, Fig. 3e). Assuming an average photoperiod of 13.5 h d^{-1}, this corresponds to an average range of 696 to 958 µmol m^{-2} s^{-1} for the shallowest plate and 357 to 544 µmol m^{-2} s^{-1} for the deepest plate. Average calculated irradiance was consistently high enough to support marine or freshwater algae growth (see review by Kirk 1994). Median PAR did not vary between early and late experiments (Table 2).

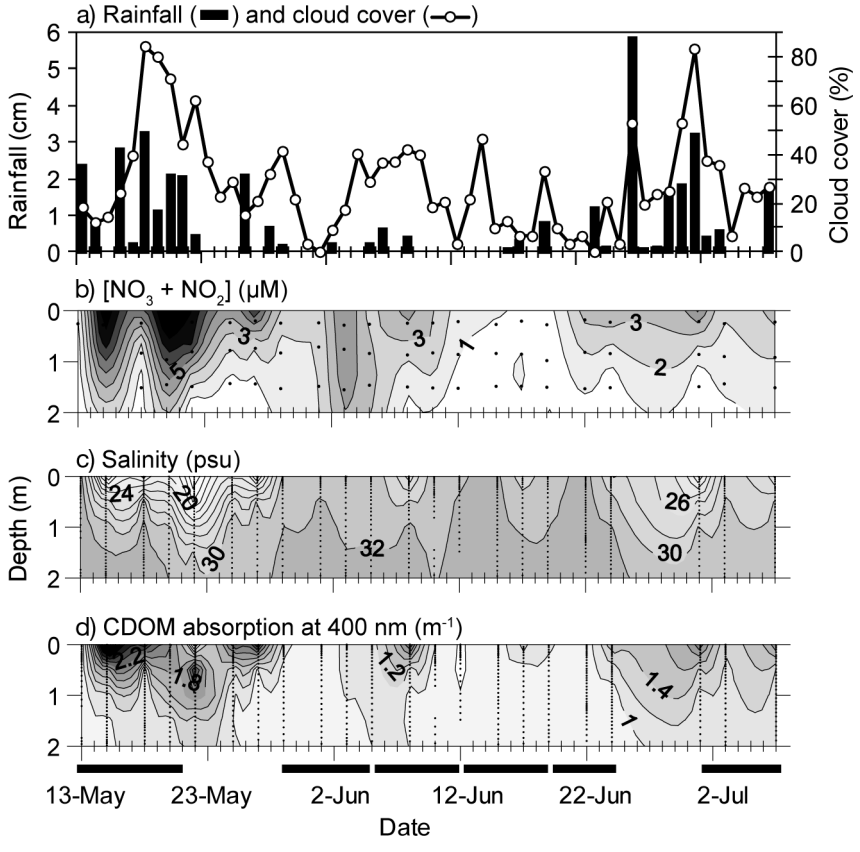

Fig. 2. (a) Daily rainfall and percent daily cloud cover during daylight hours, and depth–time kriged contours for (b) nitrate + nitrite concentrations, (c) salinity, and (d) colored dissolved organic matter (CDOM) at the experiment site. Black points within contours (b–d) identify the spatial and temporal resolution of measurements. Black bars above dates identify the durations of the 6 experiments

Growth of the microalgal community

The OM on the glass plates that was visible under light microscopy included pennate and centric diatoms, diatom mucilage, filamentous algae, and occasional cnidarian polyps; these taxa are representative of the benthic microalgal community (Cahoon 1999). During the 3 early

Table 1. Summary data for photosynthetically active radiation (PAR), organic matter accumulation rate (A_{OM}), $\delta^{13}C$ signatures of dissolved inorganic carbon ($\delta^{13}C_{DIC}$), aqueous CO_2 ($\delta^{13}C_{CO2}$), and OM ($\delta^{13}C_{OM}$), carbon isotope fractionation by organic matter (ε), and aqueous CO_2 concentration [CO_2(aq)]. PAR values are the averages of calculated daily integrated PAR. Pennate diatom cover class quantifies spatial coverage by pennate diatoms on glass slides. Water-column parameters are averages of 3 to 4 measurements made at the start, middle, and end of each experiment

Dates (2009)	Depth (m)	PAR (mol m^{-2} d^{-1})	A_{OM} (µg cm^{-2} d^{-1})	$\delta^{13}C_{DIC}$ (‰)	$\delta^{13}C_{CO2}$ (‰)	$\delta^{13}C_{OM}$ (‰)	ε (‰)	[CO_2(aq)] (µmol kg SW^{-1})	Salinity (psu)	Pennate diatom cover class (%)
13–21 May	0.2	33.8	6.55	–3.09	–11.77	–20.17	8.57	20.7	23.0	85
	0.53	28.6	4.90	–2.45	–11.12	–19.65	8.70	18.5	27.5	97.5
	0.86	24.2	3.46	–1.82	–10.47	–19.75	9.46	16.4	32.0	97.5
	1.19	20.5	2.82	–1.81	–10.47	–17.19	6.84	17.0	32.4	97.5
	1.52	17.4	2.02	–1.81	–10.46	–20.02	9.75	17.6	32.8	97.5
29 May–5 June	0.2	46.6	4.74	–2.23	–10.83	–21.38	10.78	20.0	32.0	85
	0.53	40.4	8.35	–2.17	–10.76	–20.89	10.34	19.2	32.1	85
	0.86	35.1	7.35	–2.10	–10.69	–21.61	11.15	18.3	32.1	85
	1.19	30.4	8.28	–2.04	–10.69	–20.90	10.43	18.1	32.2	85
	1.52	26.4	5.27	–2.11	–10.69	–21.19	10.73	17.9	32.4	97.5
5–12 June	0.2	39.3	1.27	–2.18	–10.68	–21.78	11.35	17.0	31.1	85
	0.53	33.9	2.45	–1.97	–10.46	–21.47	11.24	16.0	31.6	85
	0.86	29.2	1.82	–1.76	–10.24	–21.83	11.84	15.0	32.2	85
	1.19	25.2	1.45	–1.75	–10.23	–18.79	8.72	14.8	32.3	97.5
	1.52	21.7	1.70	–1.74	–10.22	–21.59	11.62	14.5	32.4	85
12–19 June	0.2	43.4	2.27	–1.96	–10.29	–23.65	13.68	17.0	32.3	15
	0.53	36.5	3.48	–1.88	–10.21	–22.08	12.14	15.6	32.3	15
	0.86	30.7	0.84	–1.79	–10.13	–20.96	11.06	14.2	32.4	62.5
	1.19	25.9	1.75	–1.80	–10.14	–21.20	11.30	14.6	32.4	62.5
	1.52	21.8	0.74	–1.80	–10.15	–18.72	8.73	15.1	32.4	62.5
19–24 June	0.2	46.1	1.62	–2.18	–10.48	–23.51	13.34	17.8	31.4	37.5
	0.53	38.4	2.32	–1.91	–10.20	–22.43	12.51	16.2	32.0	37.5
	0.86	32.1	2.36	–1.64	–9.93	–21.45	11.78	14.7	32.5	62.5
	1.19	26.7	1.73	–1.65	–9.94	–18.12	8.33	14.6	32.6	62.5
	1.52	22.3	1.35	–1.67	–9.95	–19.22	9.45	14.6	32.7	97.5
1–7 July	0.2	35.4	0.77	–2.96	–11.44	–23.46	12.31	18.7	25.8	15
	0.53	29.8	0.52	–2.61	–11.06	–22.90	12.12	17.1	28.4	37.5
	0.86	25.1	0.76	–2.27	–10.67	–22.52	12.12	15.5	30.9	37.5
	1.19	21.1	0.93	–2.21	–10.62	–22.19	11.84	15.7	31.0	37.5
	1.52	17.8	0.97	–2.16	–10.57	–22.08	11.78	15.9	31.2	37.5

experiments, the OM was dominated by pennate diatoms with small contributions by centric diatoms and filamentous algae (Fig. 3c, Table 1; algal cover classes in Table A1). During the 3 later experiments, median coverage by pennate diatoms was significantly lower (Table 2). The OM in the later experiments included more filamentous algae with minor contributions by centric diatoms and cnidarian polyps (see Table A1).

Median rates of OM accumulation were significantly higher during the early experiments, coinciding with the higher nutrient concentrations (Table 2). A_{OM} was positively correlated with [NO_3+ NO_2+NH_4] (Pearson's r = 0.47, $p < 0.01$) and with [CO_2(aq)] (Pearson's r = 0.66, $p < 0.001$). The correlation between A_{OM} and PAR was marginally insignificant (Pearson's r = 0.32, $p = 0.09$).

Carbon isotope fractionation

ε was lower during the early experiments (Table 2, Fig. 3a). During the later 3 experiments, ε was significantly higher and correlated with water depth during each experiment (Table 3). Although the early experiments had significantly higher [CO_2(aq)] and A_{OM}, ε did not correlate with [CO_2(aq)], A_{OM}, or A_{OM}/[CO_2(aq)] (all $p > 0.05$). When values were binned by A_{OM} (Fig. 4a), ε had a significant linear relationship with A_{OM}/[CO_2(aq)] within the 0–1.5 µg cm^{-2} d^{-1} category (R^2 = 0.44, $p = 0.037$). The remaining A_{OM} categories did not have significant linear or nonlinear relationships between ε and A_{OM} / [CO_2(aq)]. ε had a significant negative relationship with pennate diatom cover class (Fig. 4b). PAR had significant linear relationships with both ε (Fig. 4c) and $\delta^{13}C_{OM}$ (Fig. 4d).

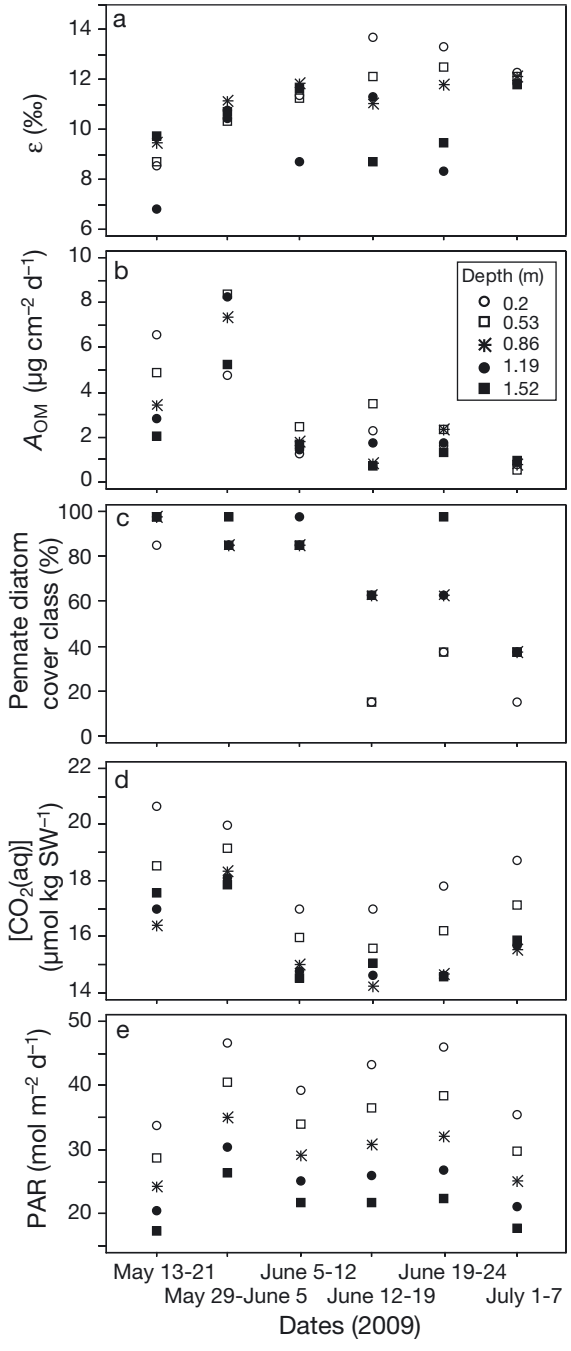

Fig. 3. (a) Carbon isotope fractionation (ε), (b) organic matter accumulation rate (A_{OM}), (c) pennate diatom cover class, (d) aqueous CO_2 concentration ([CO_2(aq)]), and (e) photosynthetically active radiation (PAR) at the 5 depths examined over the course of 6 experiments

Among the variables PAR, [NO_3+NO_2+NH_4], A_{OM}, [CO_2(aq)], and the 3 algal cover classes, the best linear multiple regression model for explaining variation in ε contained a constant and terms for variation in PAR and pennate diatom cover class (Fig. 5). This model had the lowest (best) AIC score and explained 56% of the variability in observed ε (see Fig. 5; R^2 = 0.56, adjusted R^2 = 0.53). Among the 6 models with the best AIC scores, PAR was selected in 5 cases and pennate diatom cover class was selected in all cases (Table 4). VIF was low (1.09) in the model shown in Fig. 5, indicating that multicollinearity did not substantively interfere with this relationship. PAR and pennate diatom cover class were not significantly correlated (p = 0.13). Data from the first week were omitted and the multiple regression analysis was repeated. This determined that the first week, with its associated high nutrient concentrations and low ε, was not driving the relationship. The multiple regression from this smaller data set, ε = 11.26 − 0.03 Pennate + 0.05PAR (R^2 = 0.51, p < 0.001), was similar to the regression in Fig. 5.

DISCUSSION

Dominant controls on ε

ε ranged from 6.8 to 13.7‰ among individual glass plates. Maximum ε_p has been suggested to be 25 to 28‰ (Goericke et al. 1994, Popp et al. 1998). ε_p can be much lower than these values; ε_p on the order of 6 to 13‰ is not unusual for aquatic microalgae (Hollander & McKenzie 1991, Rost et al. 2002). Bade et al. (2006) found ε_p by *in situ* freshwater algae to be in the range of 0 to 15‰.

The most parsimonious model for explaining variation in ε included pennate diatom cover class and PAR (Fig. 5). These 2 variables were consistently selected in the top 6 models with the best AIC scores (Table 4), supporting their mutual importance as predictors of ε. Variability within pennate diatom class and PAR individually explained 48 and 22% of ε variation, respectively (Fig. 4b,c). When combined as a multiple regression, these parameters explained 56% of ε variation.

As shown by the significant relationship between pennate diatom cover class and ε, variable community composition impacted community carbon fractionation in this study. Species-specific variation in ε_p due to variable rates and mechanisms of carbon uptake, membrane permeability, and cell geometry is well documented (Popp et al. 1998, Burkhardt et al. 1999). For example, ε_p values for *Emiliania huxleyi* were 8 to 10‰ lower than ε_p for *Skeletonema costatum* when grown under identical conditions (Hinga et al. 1994). Diatoms often exhibit lower photosynthetic fractionation and higher $\delta^{13}C$ values compared

Table 2. Median values of parameters during the 3 early experiments (13 May to 12 June) and 3 later experiments (12 June to 7 July). Mann-Whitney *U*-tests compare early and late median values. Parameters are defined in Tables 1 & A1

Parameter	Units	Early (n = 15)	Late (n = 15)	p	*U*
ε	‰	10.43	11.84	0.007	178.5
A_{OM}	μg cm^{-2} d^{-1}	3.46	1.35	<0.001	32.0
Pennate diatom cover class	%	85.0	37.5	<0.001	12.0
[CO_2(aq)]	μmol kg SW^{-1}	17.6	15.6	0.019	55.5
[NO_3+NO_2]	μM	2.93	0.96	<0.001	19.0
PAR	mol m^{-2} d^{-1}	29.2	29.8	0.97	114.0
Salinity	psu	32.13	32.26	0.756	120.5
CDOM D(440)	m^{-1}	1.02	0.98	0.533	97.0

to other marine algae, likely due to high growth rates and large cell sizes (Fry & Wainright 1991, Popp et al. 1998). Cyanobacteria also have particularly high $\delta^{13}C$ values as a result of their efficient uptake of HCO_3^- (Badger 2003, Ishikawa et al. 2012).

ε was significantly lower during the early experiments, which had greater coverage by pennate diatoms and higher A_{OM}, nutrient concentrations, and [CO_2(aq)] (Table 2). The 3 later experiments had lower A_{OM}, more

Table 3. Pearson's product-moment correlation coefficients between the parameters (defined in Table 1) in Fig. 3 and water depth for each of the 6 experiments. *p < 0.05

Parameter	13–21 May	29 May–5 June	5–12 June	12–19 June	19–24 June	1–7 July
ε	0.07	0.00	−0.25	−0.94*	−0.89*	−0.96*
A_{OM}	−0.98*	0.09	−0.05	−0.67	−0.40	0.72
Pennate diatom cover class	0.71	0.71	0.35	0.87	0.93*	0.71
[CO_2 (aq)]	−0.74	−0.96*	−0.95*	−0.71	−0.89*	−0.84
PAR	−1.00*	−1.00*	−1.00*	−0.99*	−0.99*	−1.00*

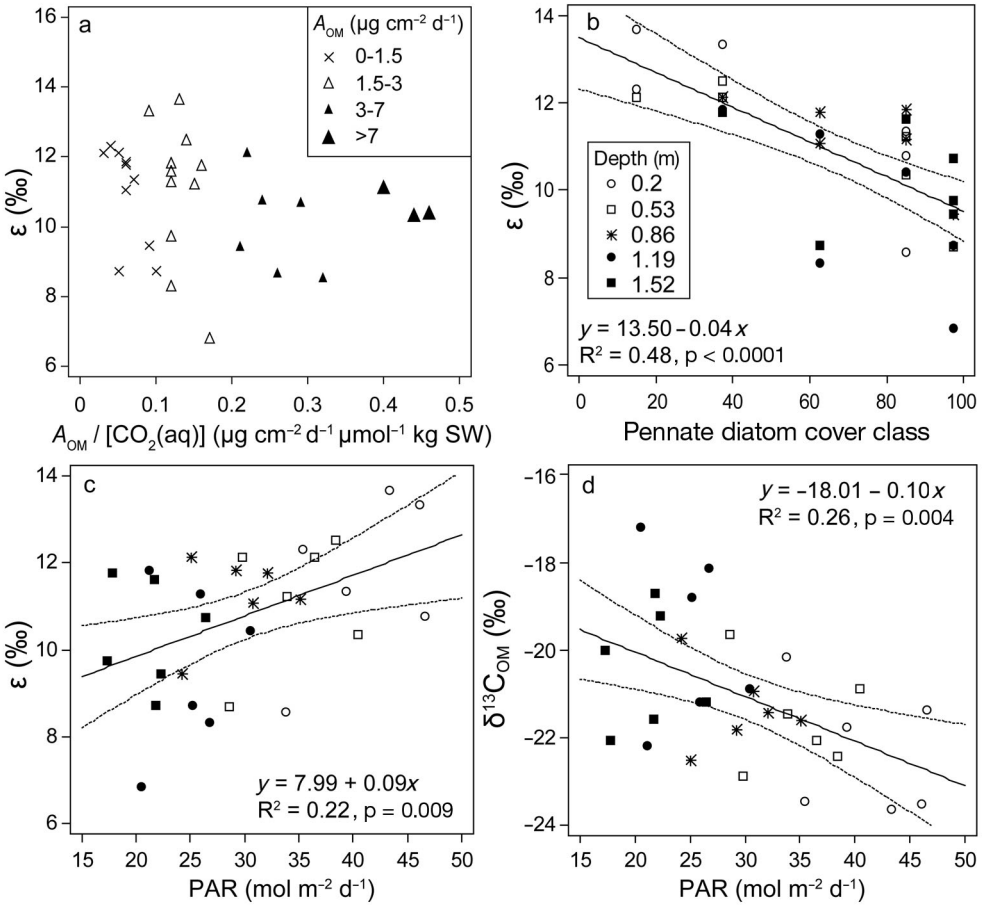

Fig. 4. Carbon isotope fractionation (ε) as a function of (a) the ratio of organic matter accumulation rate to aquatic CO_2 concentration (A_{OM})/[CO_2(aq)]. (b) spatial dominance by pennate diatoms, and (c) photosynthetically active radiation (PAR), and (d) $\delta^{13}C_{OM}$ as a function of PAR. Dotted lines indicate 95% confidence limits for estimated means

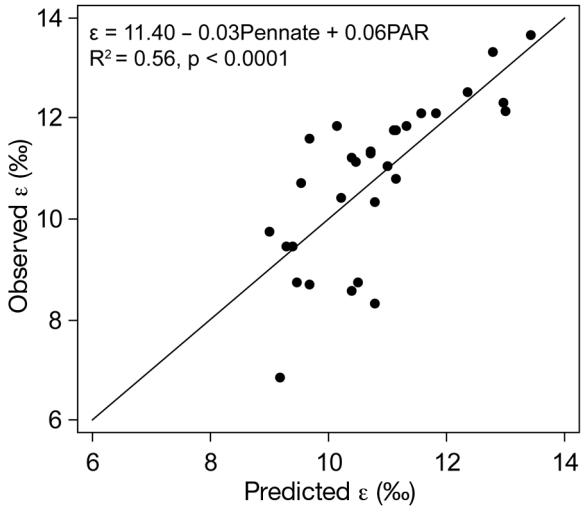

Fig. 5. Performance of a multiple regression model to predict carbon isotope fractionation of organic matter (ε) as a function of photosynthetically active radiation (PAR) and pennate diatom cover class

diverse algal assemblages, and a wider range of ε that was strongly correlated with water depth (p-values < 0.05 for the last 3 experiments, see Table 3). PAR was the only other variable that also consistently demonstrated significant correlations with water depth for the last 3 experiments (Table 3).

As previously mentioned, the relationship between PAR and photosynthetic fractionation can be difficult to detect due to correlations between growth rate and PAR and their opposing influence on fractionation (Riebesell et al. 2000, Rost et al. 2002). In our experiments, A_{OM} had a stronger correlation with nutrients and [CO_2(aq)] than with PAR, which likely facilitated our detection of the positive relationship between PAR and ε. Among individual glass plates, ε had a range of 6.84‰. While PAR was one of the strongest explanatory variables in these *in situ* experiments, the average amount of PAR-related variation in fractionation (~3‰ according to Fig. 4c) can be even greater in laboratory studies. Riebesell et al. (2000) observed a 4 to 8‰ increase in ε_p by *Phaeodactylum tricornutum* under light-saturated, nutrient-limited conditions compared to light-controlled, nutrient-replete conditions. Variation in photoperiod yielded a similarly large effect, with ε_p values 4 to 6‰ larger for diatoms grown under continuous light compared to algae grown under a 16:8 h light:dark cycle (Burkhardt et al. 1999). The range of calculated PAR reaching the glass plates (17.4 to 46.6 mol m^{-2} d^{-1} or an average photon flux density of 357 to 985 µmol m^{-2} s^{-1}) is similar to previously calculated underwater PAR for the region (Anastasiou 2009), yet the light availability for algae in this field experiment was greater than the photon flux density for laboratory experiments investigating the influence of PAR on ε_p (Burkhardt et al. 1999, Riebesell et al. 2000, Rost et al. 2002).

There are several possible explanations for the lack of a relationship between ε and A_{OM}/[CO_2(aq)] in this study (Fig. 4a). Our experiments quantified algal accumulation rates rather than specific growth rate. Therefore, the results are not quantitatively comparable to the µ/[CO_2(aq)] metric frequently used in laboratory studies. The relationship between ε_p and µ/[CO_2(aq)] is itself difficult to predict, as it varies among algal species (Popp et al. 1998). While the ε_p versus µ/[CO_2(aq)] relationship is often shown to be linear (Bidigare et al. 1997, Popp et al. 1998), some studies have found a curvilinear relationship due to the active uptake of inorganic carbon at high growth rates (Laws et al. 1997, Cassar et al. 2006). The curvilinear relationship between ε_p and µ/[CO_2(aq)] may also vary if growth is nutrient-limited or light-limited (Cassar et al. 2006). According to the model developed by Cassar et al. (2006), at any given ratio of µ/[CO_2(aq)], ε_p will be lower at high growth rates if algae are grown under nutrient-limited conditions; however, ε_p will be higher at high growth rates under light-limited conditions. Thus, it is necessary to bin data by growth rate to discern any possible relationships between ε_p and µ/[CO_2(aq)]. When the data in this study were binned by A_{OM} (Fig. 4a), only the 0–1.5 µg cm^{-2} d^{-1} category demonstrated a significant relationship (both linear and curvilinear relationships tested) between ε and A_{OM}/[CO_2(aq)]. Due to the lack of multiple A_{OM} categories at a given A_{OM}/[CO_2(aq)], it was not possible to deter-

Table 4. Mean square error (MSE) and adjusted R^2 values of best multiple regression models to predict carbon fractionation (ε) based upon lowest Akaike Information Criterion (AIC) values. Possible variables included PAR, [NO_3+NO_2+NH_4], A_{OM}, [CO_2(aq)], and cover classes for pennate diatoms, centric diatoms, and filamentous algae. Variables are defined in Table 1

Variables	AIC	ΔAIC	MSE	R^2	adj R^2
PAR, pennate	0.414	0	1.24	0.56	0.53
PAR, pennate, [CO_2(aq)]	0.459	0.045	1.21	0.58	0.54
PAR, pennate, centric	0.477	0.063	1.23	0.58	0.53
pennate	0.477	0.063	1.41	0.48	0.46
PAR, pennate, A_{OM}	0.495	0.081	1.26	0.57	0.52
PAR, pennate, [NO_3+NO_2+NH_4]	0.510	0.096	1.27	0.56	0.51

mine whether the algal growth was limited by light or nutrients based upon the model of Cassar et al. (2006).

Sources of variability in natural settings

The relatively low R^2 values for significant ε correlations (Fig. 4b,c) are likely influenced by the inherent variability of a natural setting. Stratification in the water column and the presence of a high-nutrient, high-CDOM surface layer resulted in correlations among variables, making it difficult to isolate the effects of individual parameters. Other studies in natural environments have also had difficulty predicting ε_p and deriving significant correlations due to covariation among relevant parameters (MacLeod & Barton 1998, Bade et al. 2006). Seasonal variability also impacts ε_p and $\delta^{13}C$ values of microalgae (Hollander & McKenzie 1991, Ishikawa et al. 2012). For instance, Ishikawa et al. (2012) found that freshwater periphyton had significantly higher $\delta^{13}C$ values in the winter compared to spring and summer. Hollander & McKenzie (1991) also found that the species composition, $\delta^{13}C$ values, and ε_p all varied seasonally in freshwater phytoplankton. Seasonal change was evident in the present study, which took place during the transition from the dry season to the wet season. Within 2 mo, the algal assemblage changed from one dominated by pennate diatoms to a more diverse assemblage that included centric diatoms and filamentous algae.

OM on the glass plates was exposed to grazing, which may have influenced OM biomass and A_{OM}. The plates were not covered or shielded from primary consumers to avoid barrier effects on CO_2(aq) and shading of ambient light. Filamentous algae may have caused secondary shading of other algal growth on the glass plates; this factor was not incorporated into calculations of the light environment. A_{OM} may have been impacted by the length of time the plates were left in the water if accumulation rates were exponential rather than linear. This study focused on OM larger than 35 µm; different fractionation trends may occur in the smaller size fraction due to the larger surface area to volume ratio of small cells (Popp et al. 1998). Additionally, the acidification and rinsing procedure used to remove inorganic carbon may not have completely removed all diatom mucilage or bacteria. It is possible that algal cells may have burst during this process, resulting in the loss of cellular contents. Future studies should use a different acidification process to avoid this possibility.

The lack of a significant correlation between ε and [CO_2(aq)] may also be affected by the need for higher temporal resolution when monitoring diel cycles. At a Tampa Bay location 18.5 km distant from the Bayboro Harbor site used in this study, Yates et al. (2007) observed a mean diel pCO_2 fluctuation of 218.1 µatm. Over the course of our 8 wk study, which was conducted in a more semi-enclosed location than the study of Yates et al. (2007), pCO_2 fluctuated by 353.6 µatm. With the exception of 2 days, all sampling measurements for these experiments were made between 09:00 and 11:30 h, near the daily peak in [CO_2(aq)] (Yates et al. 2007). The significant daily variation in pCO_2 documented by Yates et al. (2007) highlights the need for high-resolution sampling to accurately quantify average [CO_2(aq)].

Implications for trophic studies

The reason for the ~5‰ higher $\delta^{13}C$ values in benthic algae compared to phytoplankton is often attributed to a boundary-layer effect (Smith & Walker 1980, France 1995). In the present experiments, the OM was accumulated on glass plates; any difference in thickness of the boundary layer surrounding the plates would be the result of variable water velocity, turbulence, or thickness and texture of OM accumulations (Smith & Walker 1980, Vogel 1994, MacLeod & Barton 1998). It is possible that the shallowest plate may have been exposed to higher water velocity due to surface-water motion. However, the experiments were conducted in a sheltered harbor that was largely shielded from wind and waves. The shallowest plate, which contained the greatest accumulation of OM, may have had restricted diffusion of CO_2 due to cell overlap or mucilage buildup. However, there was no correlation between A_{OM} and ε ($p = 0.20$).

The linear relationships between both ε and $\delta^{13}C_{OM}$ with PAR in this study suggest that light limitation may significantly contribute to the observed global offset between $\delta^{13}C$ values of phytoplankton and benthic algae. $\delta^{13}C_{OM}$ values among individual glass plates varied by 6.5‰, which is greater than the average 5‰ difference between $\delta^{13}C$ values of benthic algae and phytoplankton (France 1995, Doi et al. 2010). Variability within the isotopic baseline presents challenges for trophic studies, as the ranges of $\delta^{13}C$ values for planktonic and benthic biomass may overlap, complicating calculations of basal resource use and introducing noise into isotopic mixing models (Casey & Post 2011). The observed range of variation in $\delta^{13}C_{OM}$ values reinforces the need for

adequate spatial and temporal sampling to establish the baselines used in bulk-isotope trophic studies.

SUMMARY

Carbon isotope fractionation is inherently difficult to predict for an amalgam of species in a natural setting; the best model in this study explained just 56% of variability in ε. The results presented here are consistent with light and species effects determining ε and $\delta^{13}C$ values of aquatic primary producers. The variability in the $\delta^{13}C$ values of benthic algae should be taken into consideration when interpreting $\delta^{13}C$ baseline differences between benthic and planktonic basal resources. Correlations between carbon isotope fractionation and PAR, both in the present study and in laboratory research, provide an additional explanation for the global offset between $\delta^{13}C$ values of phytoplankton and benthic algae.

Acknowledgements. We thank K. Wolfgang, R. Kitzmiller, and D. English for their assistance and expertise in the field and laboratory. R. Byrne, X. Liu, and R. Easley provided guidance in the measurement and calculation of DIC constituents. R. Masserini, M. Potter, and K. Fanning measured the seawater nutrient concentrations. E. Goddard provided expert technical oversight in the stable isotope laboratory. J. Cannizzaro provided guidance during the measurement of CDOM and chlorophyll concentrations used in our fluorometer calibrations and absorption coefficient data. J. Ivey (Florida Fish and Wildlife Conservation Commission) assisted in the calculation of light attenuation using HydroLight software. C. Hu aided in the site-specific calculation of PAR. We thank 3 anonymous reviewers for their constructive comments. This work was performed in partial fulfillment of the requirements for a doctoral degree (K.R.R.).

LITERATURE CITED

Anastasiou CJ (2009) Characterization of the underwater light environment and its relevance to seagrass recovery and sustainability in Tampa Bay, Florida. PhD dissertation, University of South Florida, Tampa, FL

Bade DL, Pace ML, Cole JJ, Carpenter SR (2006) Can algal photosynthetic inorganic carbon isotope fractionation be predicted in lakes using existing models? Aquat Sci 68: 142–153

Badger M (2003) The roles of carbonic anhydrases in photosynthetic CO_2 concentrating mechanisms. Photosynth Res 77:83–94

Bidigare RR, Fluegge A, Freeman KH, Hanson KL and others (1997) Consistent fractionation of ^{13}C in nature and in the laboratory: growth-rate effects in some haptophyte algae. Global Biogeochem Cycles 11:279–292

Burkhardt S, Riebesell U, Zondervan I (1999) Stable carbon isotope fractionation by marine phytoplankton in response to daylength, growth rate, and CO_2 availability. Mar Ecol Prog Ser 184:31–41

Burnham KP, Anderson DR (2002) Model selection and multimodel inference: a practical information-theoretic approach, 2nd edn. Springer-Verlag, New York, NY

Burns BD, Beardall J (1987) Utilization of inorganic carbon by marine microalgae. J Exp Mar Biol Ecol 107:75–86

Cahoon LB (1999) The role of benthic microalgae in neritic ecosystems. Oceanogr Mar Biol Annu Rev 37:47–86

Casey MM, Post DM (2011) The problem of isotopic baseline: reconstructing the diet and trophic position of fossil animals. Earth Sci Rev 106:131–148

Cassar N, Laws EA, Popp BN (2006) Carbon isotopic fractionation by the marine diatom *Phaeodactylum tricornutum* under nutrient- and light-limited growth conditions. Geochim Cosmochim Acta 70:5323–5335

Daubenmire RF (1959) A canopy coverage method of vegetation analysis. Northwest Sci 33:43–64

Dickson AG, Millero FJ (1987) A comparison of the equilibrium constants for the dissociation of carbonic acid in seawater media. Deep-Sea Res A 34:1733–1743

Doi H, Kikuchi E, Shikano S, Takagi S (2010) Differences in nitrogen and carbon stable isotopes between planktonic and benthic microalgae. Limnology 11:185–192

Du C (2005) Autonomous optical measurements in Bayboro Harbor (Saint Petersburg, Florida). MSc thesis, University of South Florida, Tampa, FL

Floyd DA, Anderson JE (1987) A comparison of three methods for estimating plant cover. J Ecol 75:221–228

France RL (1995) Carbon-13 enrichment in benthic compared to planktonic algae: food web implications. Mar Ecol Prog Ser 124:307–312

Freeman KH, Hayes JM (1992) Fractionation of carbon isotopes by phytoplankton and estimates of ancient CO_2 levels. Global Biogeochem Cycles 6:185–198

Fry B (1996) $^{13}C/^{12}C$ fractionation by marine diatoms. Mar Ecol Prog Ser 134:283–294

Fry B, Wainright SC (1991) Diatom sources of ^{13}C-rich carbon in marine food webs. Mar Ecol Prog Ser 76:149–157

Goericke R, Montoya JP, Fry B (1994) Physiology of isotopic fractionation in algae and cyanobacteria. In: Lajtha K, Michener RH (eds) Stable isotopes in ecology and environmental science. Blackwell Scientific Publications, Cambridge, p 187–221

Gordon HR, Morel A (1983) Remote assessment of ocean color for interpretation of satellite visible imagery, a review. Lecture notes on coastal and estuarine studies, Vol 4. Springer Verlag, New York, NY

Gordon L, Jennings JC Jr, Ross AA, Krest JM (1993) A suggested protocol for continuous flow automated analysis of seawater nutrients. In: WOCE Methods Manual 91-1, Tech Rep 93-1. College of Oceanic and Atmospheric Sciences, Oregon State University, Corvallis, OR

Haines EB, Montague CL (1979) Food sources of estuarine invertebrates analyzed using ^{13}C and ^{12}C ratios. Ecology 60:48–56

Hayes JM (1993) Factors controlling ^{13}C contents of sedimentary organic compounds: principles and evidence. Mar Geol 113:111–125

Hinga KR, Arthur MA, Pilson MEQ, Whitaker D (1994) Carbon isotope fractionation by marine phytoplankton in culture: the effects of CO_2 concentration, pH, temperature, and species. Global Biogeochem Cycles 8:91–102

Hollander DJ, McKenzie JA (1991) CO_2 control on carbon-isotope fractionation during aqueous photosynthesis: a paleo-pCO_2 barometer. Geology 19:929–932

Holm-Hansen O, Riemann B (1978) Chlorophyll *a* determi-

nation: improvements in methodology. Oikos 30:438–447
Ishikawa NF, Doi H, Finlay JC (2012) Global meta-analysis for controlling factors on carbon stable isotope ratios of lotic periphyton. Oecologia 170:541–549
Kharlamenko VI, Kiyashko SI, Imbs AB, Vyshkvartzev DI (2001) Identification of food sources of invertebrates from the seagrass *Zostera marina* community using carbon and sulfur stable isotope ratio and fatty acid analyses. Mar Ecol Prog Ser 220:103–117
Kirk JTO (1994) Light and photosynthesis in aquatic ecosystems, 2nd edn. Cambridge University Press, Cambridge
Laws EA, Bidigare RR, Popp BN (1997) Effect of growth rate and CO_2 concentration on carbon isotopic fractionation by the marine diatom *Phaeodactylum tricornutum.* Limnol Oceanogr 42:1552–1560
MacLeod NA, Barton DR (1998) Effects of light intensity, water velocity, and species composition on carbon and nitrogen stable isotope ratios in periphyton. Can J Fish Aquat Sci 55:1919–1925
McPherson BF, Miller RL (1994) Causes of light attenuation in Tampa Bay and Charlotte Harbor, southwestern Florida. Water Resour Bull 30:43–53
Mehrbach C, Culberson CH, Hawley JE, Pytkowicz RM (1973) Measurement of apparent dissociation constants of carbonic acid in seawater at atmospheric pressure. Limnol Oceanogr 18:897–907
Mobley CD, Sundman LK (2008) HydroLight 5. Sequoia Scientific, Bellevue, WA
Mook WG, Bommerso JC, Staverma WH (1974) Carbon isotope fractionation between dissolved bicarbonate and gaseous carbon dioxide. Earth Planet Sci Lett 22: 169–176
Morel A (1974) Optical properties of pure water and pure seawater. In: Jerlov NG, Nielsen ES (eds) Optical aspects of oceanography. Academic Press, New York, NY, p 1–24
O'Brien RM (2007) A caution regarding rules of thumb for variance inflation factors. Qual Quant 41:673–690
Pierrot D, Lewis E, Wallace DWR (2006) MS Excel program developed for CO_2 system calculations. ORNL/CDIAC-105a. Carbon Dioxide Information Analysis Center, Oak Ridge National Laboratory, US Department of Energy, Oak Ridge, TN
Pope RM, Fry ES (1997) Absorption spectrum (380–700 nm) of pure water. II. Integrating cavity measurements. Appl Opt 36:8710–8723
Popp BN, Laws EA, Bidigare RR, Dore JE, Hanson KL, Wakeham SG (1998) Effect of phytoplankton cell geometry on carbon isotopic fractionation. Geochim Cosmochim Acta 62:69–77
Radabaugh KR, Peebles EB (2012) Detection and classification of phytoplankton deposits along an estuarine gradient. Estuaries Coasts 35:1361–1375
Rau GH, Riebesell U, Wolf-Gladrow D (1996) A model of photosynthetic ^{13}C fractionation by marine phytoplankton based on diffusive molecular CO_2 uptake. Mar Ecol Prog Ser 133:275–285
Riebesell U, Burkhardt S, Dauelsberg A, Kroon B (2000) Carbon isotope fractionation by a marine diatom: dependence on the growth-rate-limiting resource. Mar Ecol Prog Ser 193:295–303
Rost B, Zondervan I, Riebesell U (2002) Light-dependent carbon isotope fractionation in the coccolithophorid *Emiliania huxleyi.* Limnol Oceanogr 47:120–128
Rotatore C, Lew RR, Colman B (1992) Active uptake of CO_2 during photosynthesis in the green alga *Eremosphaera viridis* is mediated by a CO_2-ATPase. Planta 188:539–545
Smith FA, Walker NA (1980) Photosynthesis by aquatic plants: effects of unstirred layers in relation to assimilation of CO_2 and HCO_3^- and to carbon isotopic discrimination. New Phytol 86:245–259
Thorp JH, Delong MD, Greenwood KS, Casper AF (1998) Isotopic analysis of three food web theories in constricted and floodplain regions of a large river. Oecologia 117: 551–563
Vogel S (1994) Life in moving fluids: the physical biology of flow, 2nd edn. Princeton University Press, Princeton, NJ
Yao WS, Byrne RH (1998) Simplified seawater alkalinity analysis: use of linear array spectrometers. Deep-Sea Res I 45:1383–1392
Yates KK, Dufore C, Smiley N, Jackson C, Halley RB (2007) Diurnal variation of oxygen and carbonate system parameters in Tampa Bay and Florida Bay. Mar Chem 104:110–124

Appendix

Table A1. Concentrations of nitrate + nitrite, ammonium, phosphate, silicate, absorption (*D*) at 400 nm by colored dissolved organic matter (CDOM), temperature, and spatial coverage by filamentous algae. Water-quality parameters are averages of 3 to 4 measurements made at the start, middle, and end of each experiment

Dates (2009)	Depth (m)	$[NO_3+NO_2]$ (µM)	$[NH_4]$ (µM)	$[PO_4]$ (µM)	[SIL] (µM)	CDOM *D*(400) (m^{-1})	Temperature (°C)	Filamentous algae cover class
13–21 May	0.2	6.07	3.25	2.33	16.74	2.59	26.93	2.5
	0.53	4.55	2.30	2.34	13.76	1.84	26.88	2.5
	0.86	3.02	1.36	2.35	10.78	1.08	26.82	2.5
	1.19	3.00	1.95	2.45	12.14	1.06	26.86	2.5
	1.52	2.97	2.54	2.54	13.50	1.04	26.91	2.5
29 May–5 June	0.2	2.98	1.52	2.50	15.26	1.02	27.72	15.0
	0.53	2.93	1.29	2.47	15.40	1.00	27.77	2.5
	0.86	2.87	1.07	2.43	15.54	0.97	27.83	2.5
	1.19	2.93	2.21	2.55	17.49	0.96	27.84	2.5
	1.52	2.98	3.36	2.67	19.44	0.95	27.85	2.5
5–12 June	0.2	2.75	0.81	2.28	7.81	1.18	28.59	2.5
	0.53	2.57	0.70	2.33	7.18	1.04	28.69	2.5
	0.86	2.39	0.59	2.39	6.55	0.91	28.79	2.5
	1.19	1.98	1.50	2.34	8.36	0.91	28.79	2.5
	1.52	1.57	2.40	2.30	10.17	0.91	28.80	2.5
12–19 June	0.2	0.76	0.72	2.64	2.54	0.98	30.24	62.5
	0.53	0.80	0.56	2.68	2.51	0.94	30.21	37.5
	0.86	0.84	0.40	2.72	2.48	0.90	30.18	15.0
	1.19	0.70	0.26	2.60	2.49	0.90	30.15	15.0
	1.52	0.56	0.13	2.48	2.49	0.90	30.12	15.0
19–24 June	0.2	2.54	2.10	2.80	5.33	1.17	30.60	62.5
	0.53	1.75	1.46	2.84	4.59	1.05	30.63	37.5
	0.86	0.96	0.82	2.87	3.85	0.93	30.65	37.5
	1.19	0.74	0.58	2.78	3.67	0.91	30.67	15.0
	1.52	0.53	0.33	2.69	3.49	0.89	30.68	2.5
1–7 July	0.2	3.42	3.04	2.83	21.24	1.62	28.90	85.0
	0.53	2.36	2.50	2.93	20.84	1.37	29.21	37.5
	0.86	1.30	1.97	3.03	20.43	1.12	29.51	15.0
	1.19	1.17	1.92	3.07	20.99	1.10	29.52	37.5
	1.52	1.04	1.88	3.10	21.55	1.08	29.53	37.5

Editorial responsibility: Graham Savidge, Portaferry, UK

Submitted: January 22, 2013; Accepted: September 11, 2013
Proofs received from author(s): December 3, 2013